AGU PUBLICATIONS

JGR

Journal of Geophysical Research: Atmospheres

RESEARCH ARTICLE
10.1002/2015JD024234

Key Points:
- Lightning fields can be significantly affected by the presence of mountainous terrain
- ToA timing errors due to propagation along mountainous terrain depend on the threshold times
- Two simplified methods are shown to reproduce the propagation time delays in mountainous terrain

Correspondence to:
F. Rachidi,
Farhad.Rachidi@epfl.ch

Citation:
Li, D., M. Azadifar, F. Rachidi, M. Rubinstein, G. Diendorfer, K. Sheshyekani, Q. Zhang, and Z. Wang (2016), Analysis of lightning electromagnetic field propagation in mountainous terrain and its effects on ToA-based lightning location systems, *J. Geophys. Res. Atmos.*, *121*, 895–911, doi:10.1002/2015JD024234.

Received 17 SEP 2015
Accepted 25 DEC 2015
Accepted article online 3 JAN 2016
Published online 27 JAN 2016

Analysis of lightning electromagnetic field propagation in mountainous terrain and its effects on ToA-based lightning location systems

Dongshuai Li[1,2], Mohammad Azadifar[2], Farhad Rachidi[2], Marcos Rubinstein[3], Gerhard Diendorfer[4], Keyhan Sheshyekani[5], Qilin Zhang[1], and Zhenhui Wang[1]

[1]Collaborative Innovation Center on Forecast and Evaluation of Meteorological Disasters, CMA Key Laboratory for Aerosol-Cloud-Precipitation, Nanjing University of Information Science and Technology, Nanjing, China, [2]Electromagnetic Compatibility Laboratory, Swiss Federal Institute of Technology in Lausanne, Lausanne, Switzerland, [3]Institute for Information and Communications Technologies, University of Applied Sciences Western Switzerland, Yverdon-les-Bains, Switzerland, [4]Department Austrian Lightning Detection and Information System, OVE Service GmbH, Vienna, Austria, [5]Electrical and Computer Engineering Department, Shahid Beneshti University, Tehran, Iran

Abstract In this paper, we analyze the propagation effects on lightning-radiated electromagnetic fields over mountainous terrain by using a three-dimensional (3-D) finite difference time domain (FDTD) method. We also discuss the time delay error in the time-of-arrival (ToA) technique currently used to locate lightning in detection networks, specifically. Furthermore, the accuracy of different approximate methods presented in the literature is discussed and tested by using our 3-D FDTD method. It is found that (1) the time delays and amplitudes of the lightning-radiated electromagnetic fields can be significantly affected by the presence of a mountainous terrain and associated diffraction phenomena; (2) for a finitely conducting ground, the time delay shows a slight increase with the increase of the observation distance, but the time delay resulting from the finite ground conductivity appears to be smaller than that caused by the mountainous terrain; and (3) the timing error associated with the ToA technique depends on the threshold times. Threshold times of 10% and 20% of the peak provide very similar results compared to those corresponding to the peak of the first derivative of the magnetic field, and the threshold time exceeds 50% of the initial rising amplitude of the signal. Furthermore, we have assessed the accuracy of two simplified methods (terrain-envelope method and tight-terrain fit method) to account for the time delays resulting from the propagation in a mountainous terrain. It is found that both methods result in time delays that are in reasonable agreement but always overestimating the results obtained using the full-wave 3-D FDTD approach for the perfectly conducting ground. These two methods represent interesting alternatives to account for the time delay over a nonflat terrain using the terrain model.

1. Introduction

Lightning location systems (LLS) are widely used all over the world. In these systems, electric and/or magnetic field sensors in the VLF, LF, or VHF frequency ranges are employed to measure lightning-radiated electromagnetic fields for locating the lightning strike point by using different algorithms, such as magnetic direction finding (MDF), time-of-arrival (ToA), or a combination of both (MDF/ToA) [*Cummins et al.,* 2010; *Diendorfer*, 2007]. In the ToA technique, each sensor determines the time of arrival of the stroke radiated field pulse using a global positioning system (GPS) synchronized clock with a time error of typically less than 300 ns. The data from different sensors are then transferred to a position analyzer to evaluate the strike point location and the time of the discharge [*Cummins et al.,* 1998, 2010; *Schulz*, 1997; *Schulz and Diendorfer*, 2000]. The accuracy of the lightning location can be improved by correcting by refining the algorithms that determine the arrival time of an electromagnetic pulse at each sensor [*Honma et al.*, 1998; *Passi and López*, 1989; *Schulz and Diendorfer*, 2000].

Different studies have shown that the accuracy of the location obtained by using the ToA technique might be affected by effects resulting from field propagation over ground of finite conductivity [e.g., *Caligaris et al.,* 2008; *Cooray*, 2009; *Cooray et al.,* 2000; *Delfino et al.,* 2008; *Rubinstein*, 1996; *Shoory et al.,* 2011]. The finite ground conductivity affects essentially the early time response of lightning-radiated fields by attenuating its peak and slowing down its risetime. To minimize the effect of the lossy ground, several methods have been suggested for the determination of the time of arrival associated with a measured waveform [e.g., *Cooray*, 1987; *Honma et al.,* 1998].

The effect of the propagation of lightning electromagnetic fields over a rough surface has recently been taken into account by *Zhang et al.* [2012a] who analyzed the propagation effects of a fractal rough ground surface on the vertical electric field generated by lightning return strokes. They found that frequencies higher than about 2 MHz are significantly attenuated by a rough ground with a root-mean-square height of 10 m. Even for the case of propagation over sea with much higher conductivities (4 S/m or so), *Cooray and Ming* [1994] and *Zhang et al.* [2012b] also found significant attenuation of frequencies higher than about 10 MHz that are caused by the rough ocean surface. *Li et al.* [2013, 2014] analyzed the propagation effect over a rough ground on the lightning horizontal field by using the finite difference time domain (FDTD) method and found that the effect of the surface roughness on the horizontal field cannot be ignored even within distances of 100 m from the lightning channel, an increase of the land roughness resulting in a lower magnitude of the horizontal field waveform. *Paknahad et al.* [2014] studied the effect of a nonflat lossy ground on the lightning electromagnetic fields as well as the associated induced voltages on overhead lines, showing that all components of the lightning electromagnetic fields are affected by a nonflat ground configuration. *Schulz and Diendorfer* [2000] have attempted to consider a real terrain model by evaluating the length of the propagation path using the terrain model, correcting the time errors related to the signal path elongation. They noted that the location accuracy of the lightning location could be improved after considering such correction. More recently, *Li et al.* [2015] have presented a preliminary analysis on the propagation effects along hilly terrain on lightning magnetic fields by using FDTD method and noted that the waveshape, peak value, and time delay of the magnetic fields can be significantly affected when propagating along a hilly terrain.

In this paper, we will analyze the propagation effects of lightning-radiated electromagnetic fields over mountainous terrain by using a full-wave approach based on a three-dimensional (3-D) finite difference time domain (FDTD) method and discuss the timing error associated with the ToA technique in lightning location systems (LLS). Finally, we will compare the results from different approximate methods presented in the literature and validate their accuracy by using our full-wave FDTD method.

2. Estimation of Timing Error Related to the TOA Technique Resulting From Propagation Over Mountainous Terrain

The time of arrival of a measured signal used by the TOA technique for calculating the lightning location can be evaluated using different methods [e.g., *Lojou et al.*, 2011; *Schulz*, 1997]. Recently improved methods for the determination of the onset time have been introduced [*Honma et al.*, 2013] resulting in better location accuracy.

The definition of the onset time t_{on} presented by *Schulz* [1997] used in this paper is illustrated in Figure 1. It is calculated from the time t_T at which the signal exceeds a threshold E_{th}, the peak time t_p, the threshold value E_{th}, and the peak value of the signal E_p using the following expression:

$$t_{on} = t_p - \frac{t_p - t_T}{E_p - E_{th}} E_p \tag{1}$$

3. Adopted Models and Methods for the Analysis

3.1. Geometry

The configuration of the problem for evaluating the lightning-generated electromagnetic fields is illustrated in Figure 2. For the analysis, we have considered a pyramidal mountain of different heights. The base of the mountain is $L_m \times L_m$. Note that a fixed value of $L_m = 1000$ m is considered in this work. The height of the mountain was varied considering different pyramid angles α (see Figure 2), namely $\alpha = 0°$ (flat ground), 30° ($H_m = 290$ m), 45°($H_m = 500$ m), and 60°($H_m = 870$ m). Three observation points are considered in the analysis (see Figure 2): (1) Point A located at a distance d_A to the left edge of the mountain, (2) Point B located at a distance d_B to the right edge of the mountain, and (3) Point O located on the top of the mountain.

Note that all the observation points are located at a height of 10 m above the ground. It is worth noting, however, that the vertical electric and azimuthal magnetic fields do not feature a significant variation when the height of observation varies from 0 to 20 m.

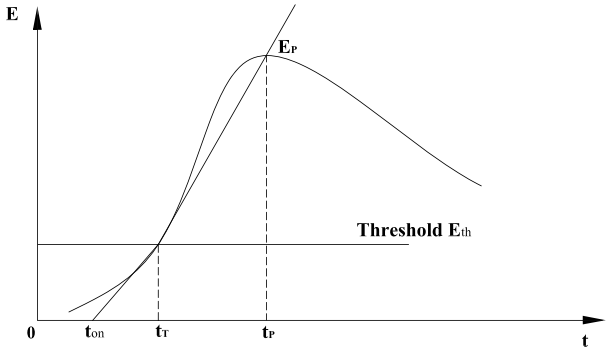

Figure 1. Calculation of the signal onset time t_{on}.

Figure 2a presents the top view of the considered geometry. For relatively close distances (up to about 1 km) between the lightning channel and the observation points, the 3-D FDTD method can directly be used for the computation of the generated electromagnetic fields (see Figure 2b in which the side view along the BB′ plane is shown). For farther distances, however, a direct 3-D FDTD approach would require prohibitive computation time and memory requirements (see *Baba and Rakov* [2014] for a review on the applications of the FDTD method to lightning electromagnetic field simulations). In order to cope with this problem and to consider in our analysis distant observation points which are relevant to lightning location systems, we have considered a plane wave representation for the lightning-generated fields for observation points beyond 50 km (see Figure 2c). The implementation of this method into the 3-D FDTD algorithm will be described in section 3.3.

It is worth noting that beyond 50 km or so, the electromagnetic field generated by a lightning channel is dominated by its radiation component; and therefore, it can be represented by a plane wave. Figure 3 shows, as an example, the waveforms of vertical electric and azimuthal magnetic fields at different distances (1 km, 50 km, and 100 km). The computations are performed assuming a perfectly conducting, flat ground and adopting the lightning channel parameters described in section 3.2. We have also represented in the same

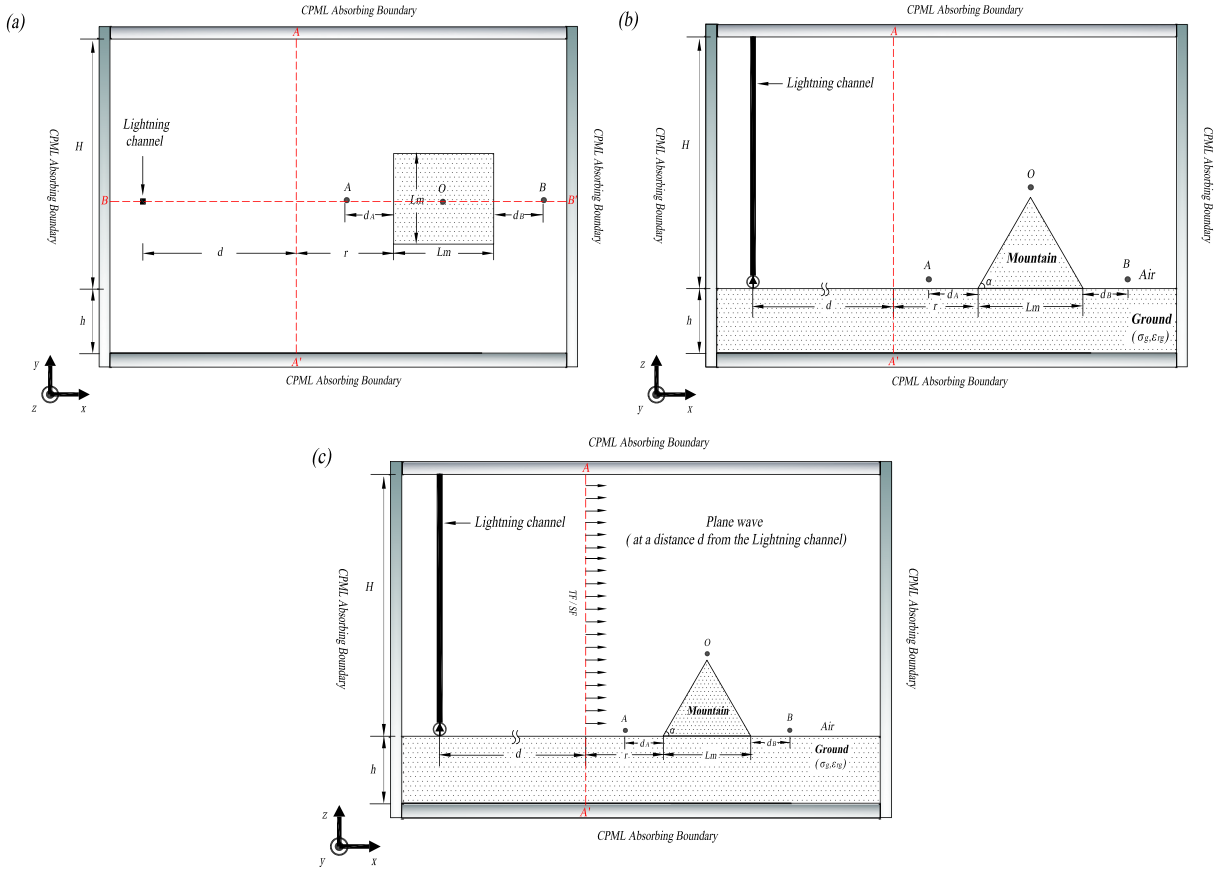

Figure 2. Geometry for the evaluation of lightning electromagnetic fields over a mountainous terrain by using 3-D FDTD: (a) top view, (b) side view BB′ in the near-field region, and (c) side view BB′ in the far-field region.

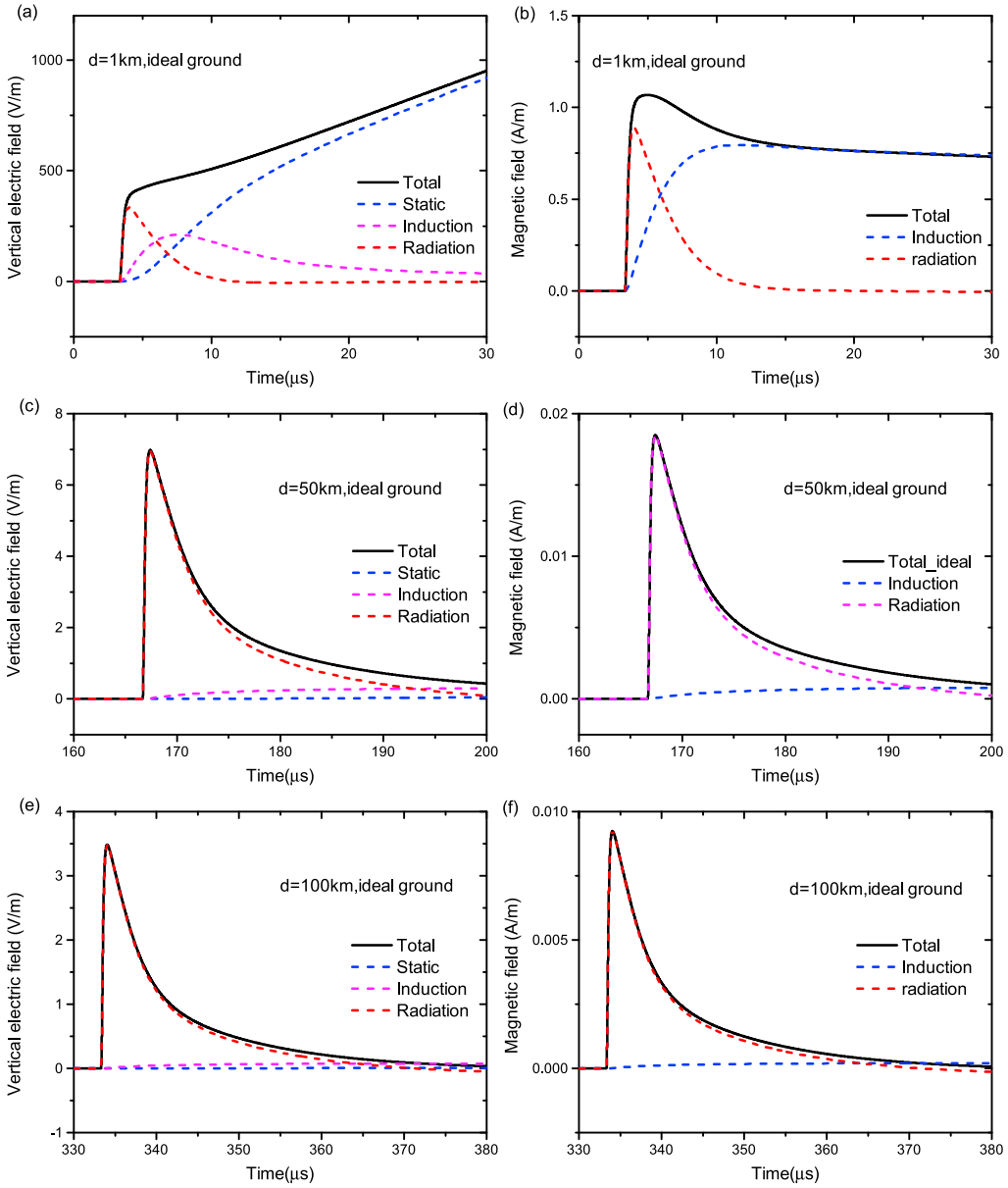

Figure 3. Electric and magnetic fields at different distances from a vertical lightning channel above a flat, perfectly conducting ground. The contribution of the different components of the fields is also shown in the figures. The adopted model and parameters are those described in section 3.2. (a and b) 1 km, (c and d) 50 km, (e and f) 100 km. Figures 3a, 3c, and 3e are the electric field. Figures 3b, 3d, and 3f are the magnetic field.

figures the contributions of various field components, namely electrostatic, induction, and radiation for the E field and induction and radiation for the H field, which are obtained through closed-form equations derived in *Uman et al.* [1975]. As can be seen from these results, for distances beyond 50 km, the electromagnetic field is essentially a plane wave: the electric and magnetic fields are characterized by similar waveshapes dominated by the radiation component, and the ratio of the two fields is given by the wave impedance.

3.2. Lightning Channel Modeling

The lightning channel is represented by a vertical array of current sources in the FDTD calculations [*Baba and Rakov*, 2003; *Li et al.,* 2014]. The current distribution along the return stroke channel is the Modified Transmission Line model with Exponential Decay [*Nucci et al.,* 1988], assuming a current decay constant $\lambda = 2000$ m [*Nucci and Rachidi*, 1989; *Rachidi and Nucci*, 1990]. The channel height is assumed to be $H = 7.5$ km

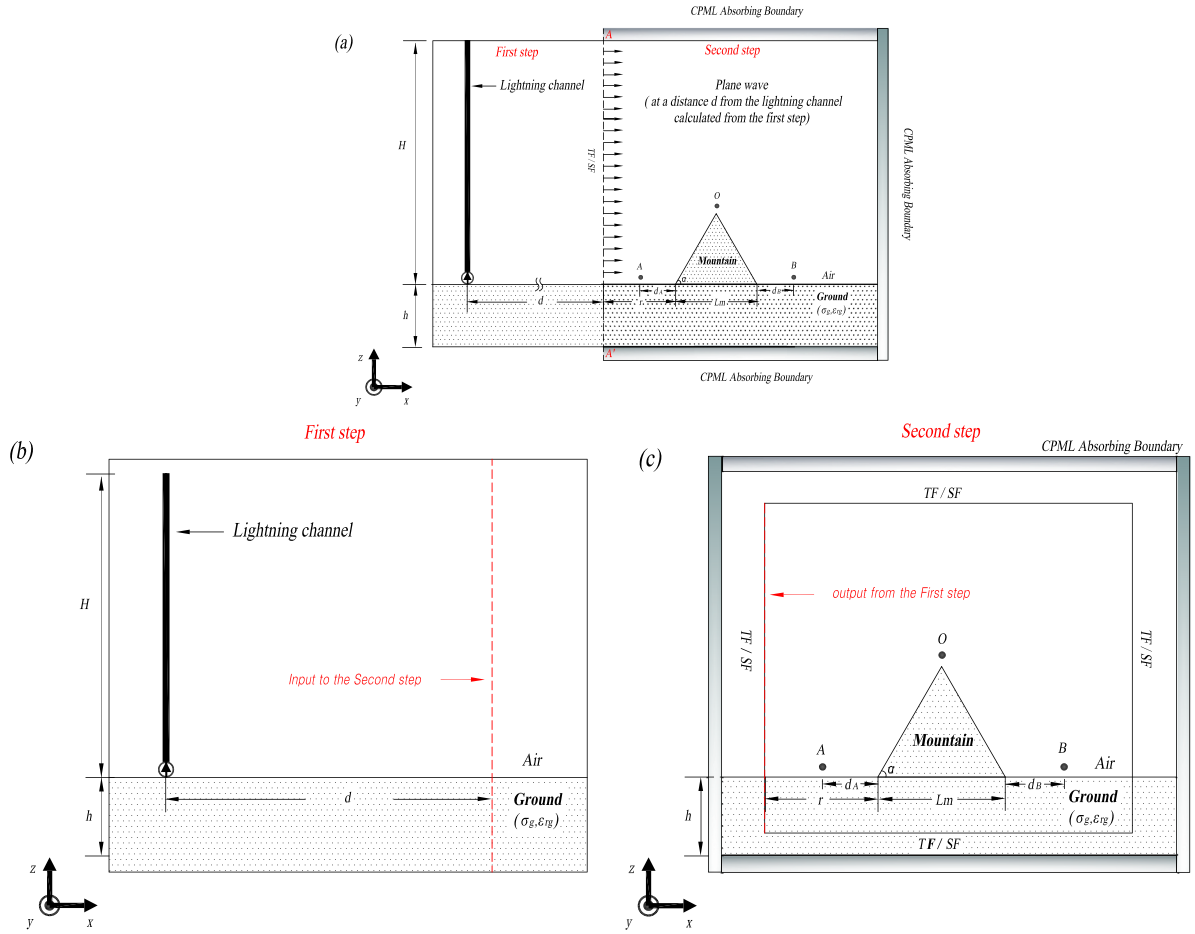

Figure 4. Plane wave representation of lightning electromagnetic fields at distant observation points. (a) Initial geometry. (b) First step in which the incident fields are evaluated in absence of the mountain. (c) Second step in which the computed fields in the previous step are injected into a constrained domain around the mountain, and the fields are evaluated at the desired observation points.

and the return stroke speed is $v = 1.5 \times 10^8$ m/s. The channel base current is represented using Heidler's functions and corresponds to typical subsequent strokes with a peak value of 12 kA and a maximum rate of rise of 40 kA/μs (the parameters can be found in *Rachidi et al.* [2001]).

3.3. 3-D FDTD Computational Parameters

Lightning electromagnetic fields were evaluated using the 3-D FDTD approach for the geometry of Figure 2 for distances of about 1 km.

The working space of 3-D FDTD is 5001 m × 3001 m × 8001 m, which is divided into cubic cells of $\Delta x \times \Delta y \times \Delta z = 10\,\text{m} \times 10\,\text{m} \times 10\,\text{m}$. The time increment is set to 19 ns. Note that the reason for the use of a spatial step of 10 m is the limited memory of the personal computer used in this work. The stair-stepping effect has been evaluated by comparing results obtained using spatial steps of 2 m, 5 m, and 10 m, which are presented in Appendix A. It can be seen that the accuracy of the numerical results with a spatial step of 10 m is acceptable for observation points in the vicinity of the mountain (A and B). On the top of the mountain, differences of up to about 20% are observed in the amplitude of the E field evaluated with different spatial steps. These differences are essentially due to the electrostatic term of the electric field, and it can be therefore expected that they will diminish at farther distances. Indeed, the magnetic field appears to be nearly invariant when the spatial step is reduced from 10 m down to 2 m.

In order to avoid reflections at the outer boundaries, we adopted six planes of the convolutional perfectly matching layers as the absorption boundary condition [*Roden and Gedney*, 2000].

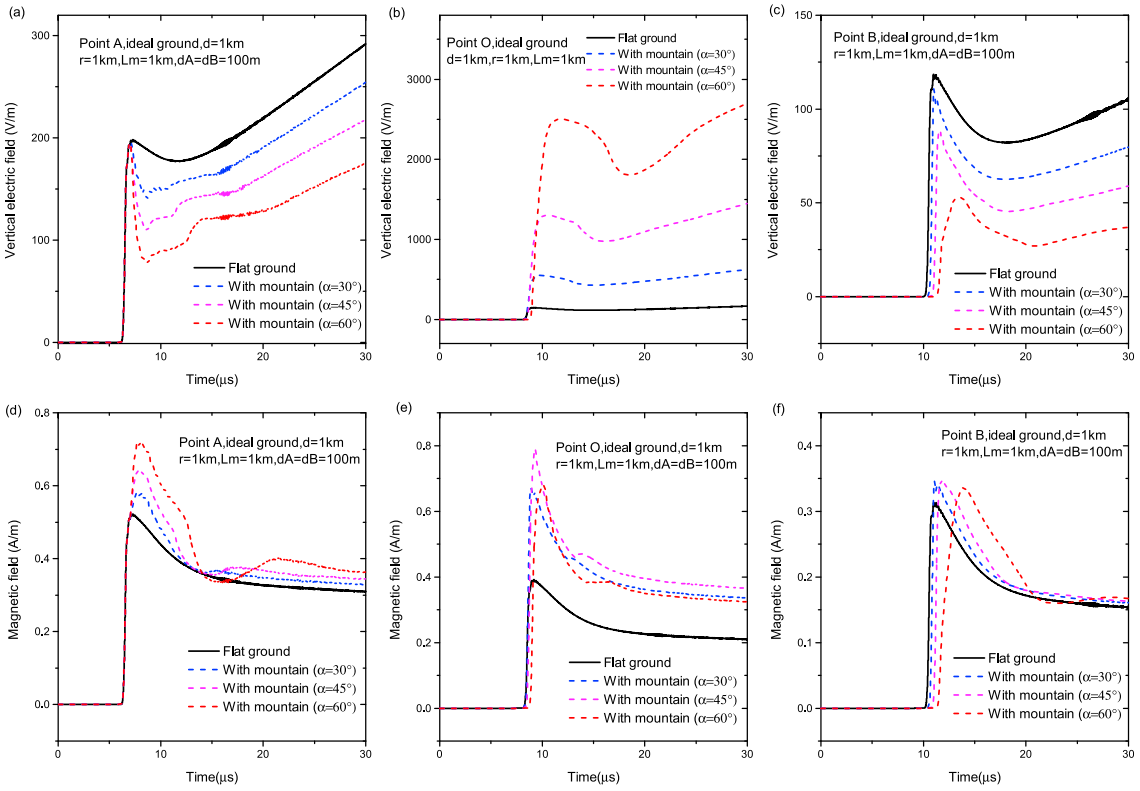

Figure 5. (a–c) Lightning vertical electric fields and (d–f) azimuthal magnetic fields at the three observation points (A, O, and B) over a height of 10 m. $d = 1$ km, perfectly conducting ground. Black solid lines, flat ground; blue dashed lines, $\alpha = 30°$; pink dashed lines, $\alpha = 45°$; and red dashed lines, $\alpha = 60°$. $d_A = 100$ m, $d_B = 100$ m.

The air, ground, and mountain are all split by Yee's grid units [*Taflove and Hagness*, 2005]. The ground and mountain are characterized by a conductivity σ_g and a relative permittivity ε_{rg}.

For farther distances (50 and 100 km), a plane wave representation of the lightning-radiated electromagnetic field was considered. For this purpose, we employed the one-dimensional incident field array with the total-field and scattered-field boundary [*Taflove and Hagness*, 1995; *Watts*, 2003] to inject plane waves into the computational domain. The approach is illustrated in Figure 4. Figure 4a presents the initial geometry in which the mountain is located at a distant location from the lightning channel. The approach consists in computing in a first step the incident fields at a distance d from the lightning channel (values of 50 and 100 km will be considered) by using closed-form expressions of the electromagnetic fields in which the effect of the finite ground conductivity is included using correction factors introduced by Wait [see e.g., *Shoory et al.*, 2012]. These fields are evaluated in absence of the mountain (Figure 4b). In a second step, the computed fields are injected as plane waves into a constrained domain around the mountain and the fields are evaluated at the desired observation points (A, B, and O) (Figure 4c).

It is worth noting that our 3-D FDTD has been tested and validated by comparing its results with those obtained using a finite element method approach, and excellent agreement has been obtained [*Li et al.*, 2015; *Paknahad et al.*, 2014].

4. Results and Analysis

4.1. Electromagnetic Fields

The vertical electric field and azimuthal magnetic field were evaluated at the three different observation points A, O, and B (see Figure 2) and considering different angles for mountain ($\alpha = 30°$, 45°, and 60°).

Figures 5–7 show, respectively, the computed waveforms of the vertical electric fields and the azimuthal magnetic fields at the three considered observation points on a perfectly conducting ground with $d_A = d_B = 100$ m, considering (i) $d = 1$ km, (ii) $d = 50$ km, and (iii) $d = 100$ km. The computations were performed

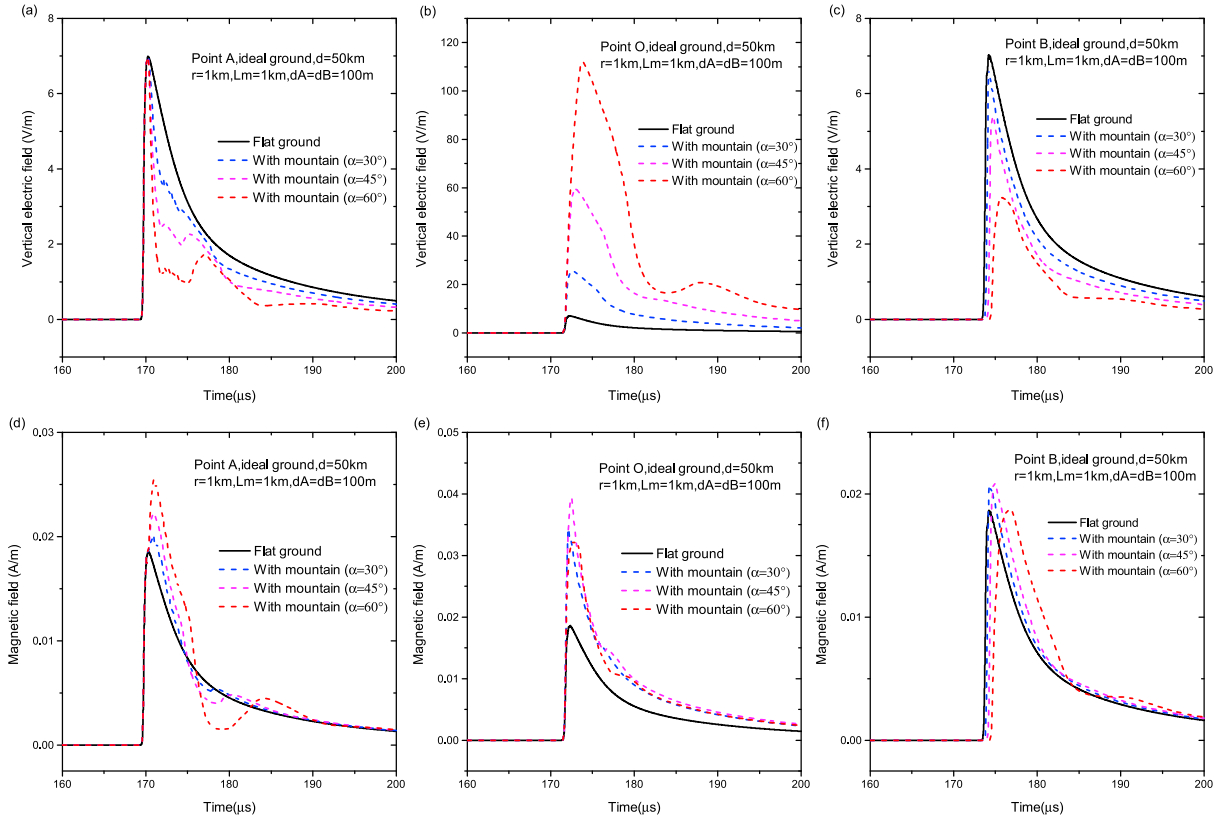

Figure 6. (a–c) Lightning vertical electric fields and (d–f) azimuthal magnetic fields at the three observation points (A, O, and B) over a height of 10 m. $d = 50$ km, perfectly conducting ground. Black solid lines, flat ground; blue dashed lines, $\alpha = 30°$; pink dashed lines, $\alpha = 45°$; and red dashed lines, $\alpha = 60°$. $d_A = 100$ m, $d_B = 100$ m.

assuming a perfectly conducting ground. It can be seen that the waveshape, amplitude, and time delays of the electromagnetic fields can be significantly affected by the presence of the mountain and associated diffraction phenomena. Also, despite the perfect ground condition, the time delay caused by the mountain on the electromagnetic fields cannot be ignored. It can be further noted that for observation points located between the lightning channel and the mountain (A) and on top of the mountain (O) the mountain has no or little effect on the time delay of the electromagnetic field. On the other hand, for an observation point behind the mountain (B), the time delay of the electromagnetic field increases with the angle of the mountain. It is interesting to note that the time delay caused by the mountain is not much influenced by the horizontal distance d to the lightning channel. Table 1 summarizes the peak value of the lightning vertical electric fields and azimuthal magnetic fields over a perfectly conducting ground at the observation point B. It can be noted that the amplitude of the electric field decreases with the angle of the mountain. On the other hand, the mountain has little effect on the peak value of the magnetic field.

In addition and as expected, the magnitude of the electric field at the top of the mountain (Point O) becomes significantly larger as the angle of the mountain increases, irrespective of the distance from the channel. The same increase can also be observed for the magnetic field for angles up to about $\alpha = 45°$, beyond which it follows a slightly decreasing trend (see Figures 5e, 6e, and 7e). It is interesting to observe that a similar behavior was reported in a recent study by *Paknahad et al.* [2014], in which the effect of a nonflat lossy ground on the lightning electromagnetic fields as well as the associated induced voltages on overhead lines was analyzed using a full-wave finite element approach. *Paknahad et al.* [2014] showed that the azimuthal magnetic field features a similar behavior as in our case, namely an increase with an increasing steepness of the nonflat surface up to a certain value (of about 60° or so), followed by a decreasing trend. In Appendix B, we have used a very simple model in an attempt to shed some light on this behavior of the magnetic field.

It is also interesting to note that at Point B (behind the mountain), the electric field decreases substantially as the angle α increases, as a result of the shielding effect of the mountain.

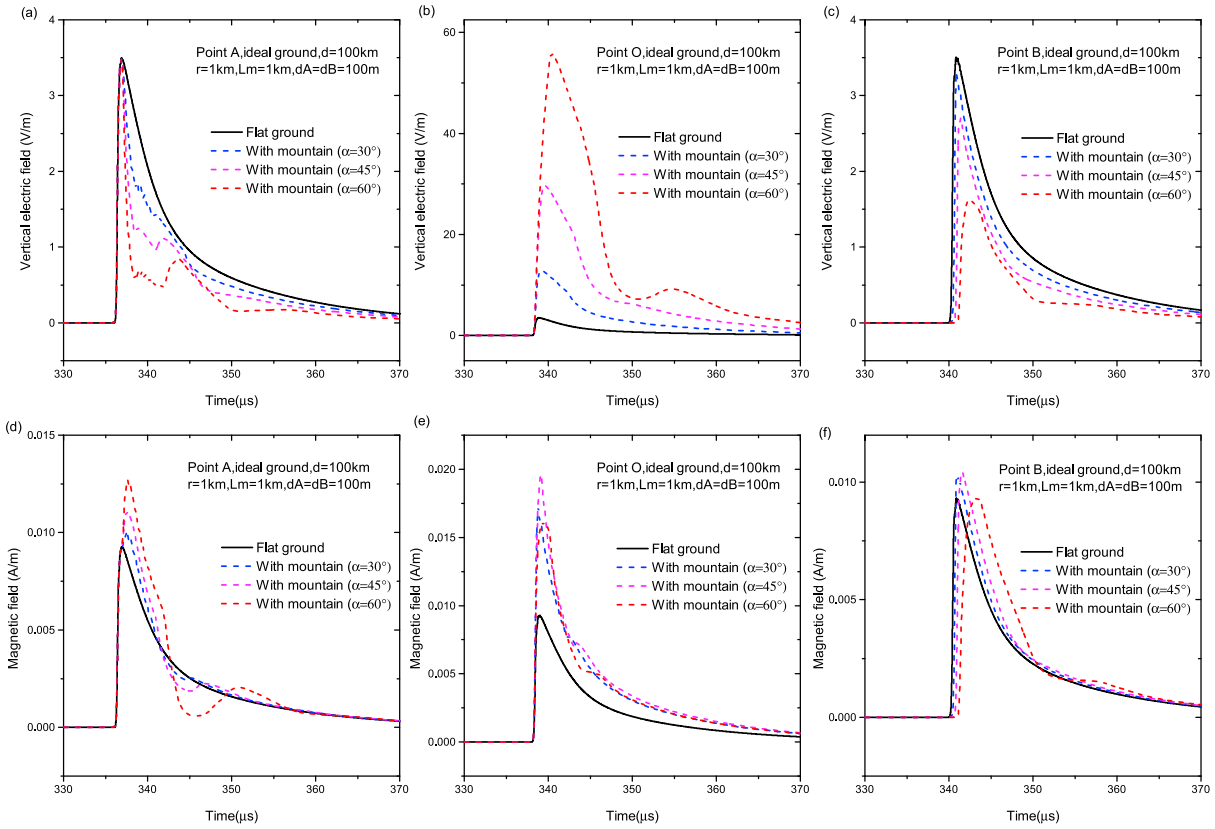

Figure 7. (a–c) Lightning vertical electric fields and (d–f) azimuthal magnetic fields at the three observation points (A, O, and B) over a height of 10 m. $d = 100$ km, perfectly conducting ground. Black solid lines, flat ground; blue dashed lines, $\alpha = 30°$; pink dashed lines, $\alpha = 45°$; and red dashed lines, $\alpha = 60°$. $d_A = 100$ m, $d_B = 100$ m.

The effect of the horizontal distance d_A and d_B is illustrated in Figure 8, in which the electric fields at points A (a, c, and e) and B (b, d, and f) at distances $d = 1$ km, 50 km, and 100 km are evaluated by increasing d_A and d_B to 500 m. It can be seen that the mountain has a reduced effect on the magnitude of the electric fields for a larger horizontal distance between the mountain and the observation points. However, the time delays at the observation point behind the mountain (point B) are not much influenced by the horizontal distance d_B.

The effect of the ground conductivity and mountain conductivity are illustrated in Figure 9, in which the lightning electromagnetic fields at point B are plotted considering (i) a perfectly conducting ground and (ii) a finitely conducting ground with a conductivity $\sigma_g = 0.001$ S/m and a relative permittivity $\varepsilon_{rg} = 10$. It can be

Table 1. Peak Values of Lightning Vertical Electric Fields and Azimuthal Magnetic Fields Over Perfectly Conducting Ground at Observation Point B

d	Angle of the Mountain	Peak Value of E (V/m)	Peak Value of H (mA/m)
1 km	0°	126.7	313.7
	30°	111.2	346.1
	45°	88.6	347.8
	60°	52.8	335.9
50 km	0°	7.0	18.7
	30°	6.6	20.6
	45°	5.4	20.9
	60°	3.2	18.7
100 km	0°	3.5	9.3
	30°	3.3	10.3
	45°	2.7	10.4
	60°	1.6	9.3

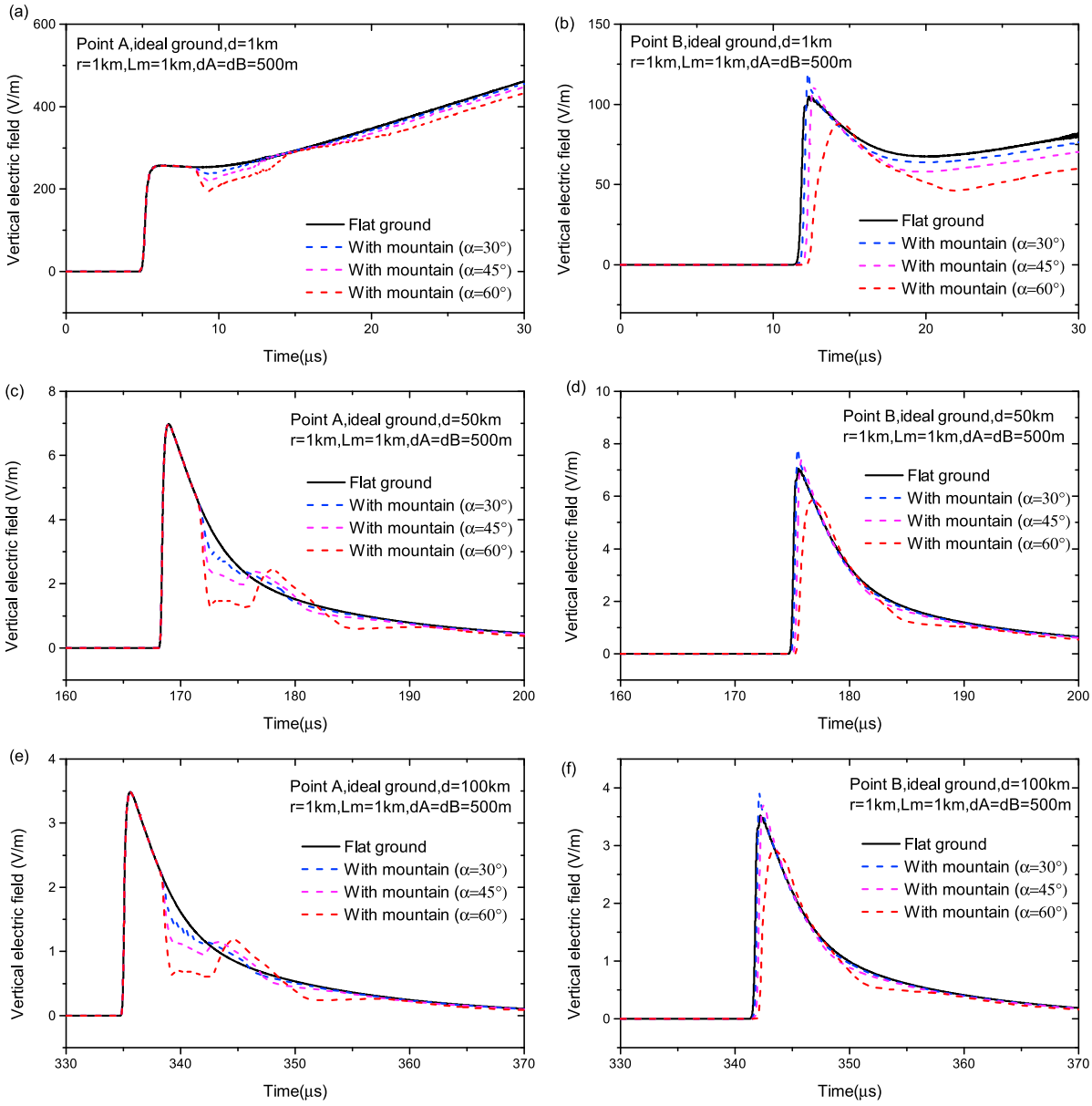

Figure 8. Lightning vertical electric fields at observation points (a, c, e) A and (b, d, f) B for $d_A = d_B = 500$ m. $d = 1$ km (Figures 8a and 8b), $d = 50$ km (Figures 8c and 8d), $d = 100$ km (Figures 8e and 8f). Perfect ground. Black solid lines, flat ground; blue dashed lines, $\alpha = 30°$; pink dashed lines, $\alpha = 45°$; and red dashed lines, $\alpha = 60°$.

seen that the effect of the presence of the mountain on the amplitude of the electromagnetic fields does not significantly depend on the ground conductivity. Note that in the near-field region ($d = 1$ km), the finite ground conductivity results in a slight decrease of the amplitude and time delays of the electromagnetic fields. However, in the far-field region ($d = 50$ km and $d = 100$ km), the time delay at point B appears to increase when taking into account the finite ground conductivity, which results in an increase in the risetime. It is interesting to note that in the near-field region, the effect of the mountain on the fields is much more pronounced than the effect of the finite ground conductivity. However, in the far-field region (50 km and beyond), the effect of the finite ground conductivity cannot be ignored.

4.2. Resulting Errors in ToA-Based Lightning Location Systems

In this section, we discuss the resulting errors in the evaluation of the arrival time related to the ToA technique. To evaluate the time delay errors of the ToA technique originated from the presence of the mountain, we calculated the onset time t_{on} by using equation (1), in which the involved parameters (t_p, E_p, t_T) were

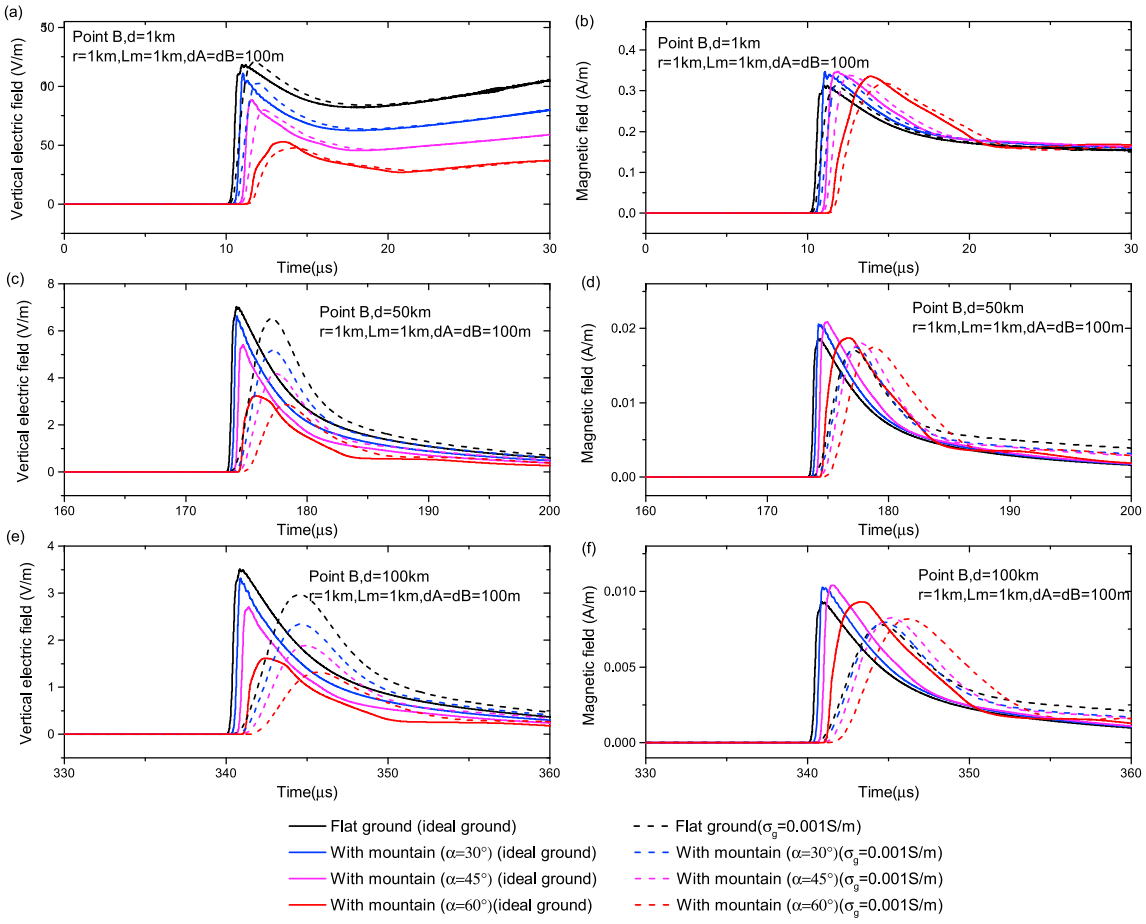

Figure 9. (a,c,e) Lightning vertical electric fields and (b, d, f) azimuthal magnetic fields over perfectly conducting ground (solid line) and finitely conducting ground with $\sigma_g = 0.001$ S/m and $\varepsilon_{rg} = 10$ (dashed line) at observation point B.

extracted from the numerical results obtained using our 3-D FDTD approach. The calculations were performed for three different observation points (A, O, and B) and for different ground/mountain electrical parameters (perfect ground and $\sigma_g = 0.001$ S/m, $\varepsilon_{rg} = 10$). The onset time t_{on} was calculated from the azimuthal magnetic field by using equation (1).

In order to compare the results from different approximation methods presented in the literature [*Cooray*, 1987; *Honma et al.,* 1998; *Schulz and Diendorfer*, 2000], we will consider four different values for the threshold time t_T to calculate the onset time t_{on}, which are the times corresponding to (1) 10% of the initial rising amplitude of the magnetic field, (2) 20% of the initial rising amplitude of the magnetic field, (3) 50% of the initial rising amplitude of the magnetic field [*Cooray*, 1987], and (4) the peak of the first derivative of the magnetic field [*Cooray*, 1987].

Additionally, the delays corresponding to speed-of-light propagation along two different elongated propagation paths, namely the terrain-envelope method (marked by the blue line in Figure 10), and tight-terrain fit method (marked by the red line in Figure 10) were considered and were compared with the results of FDTD method. Note that the tight-terrain fit method corresponds to the approach proposed by *Schulz and Diendorfer* [2000]. Figure 11 shows the time delay calculated making use of the onset time t_{on} and considering different threshold times t_T, and the two different elongated propagation path methods, assuming the ground and the mountain as perfect conductors. Figure 12 present the results for the time delays taking into account the finite ground conductivity for $\sigma_g = 0.001$ S/m with $\varepsilon_{rg} = 10$. In each figure, the results are presented at observation point B considering different angles for the mountain.

It can be noted that the onset time t_{on} is strongly affected by the presence of the mountain, both for a perfectly conducting ground/mountain and for a finitely conducting ground and mountain. Specifically, it

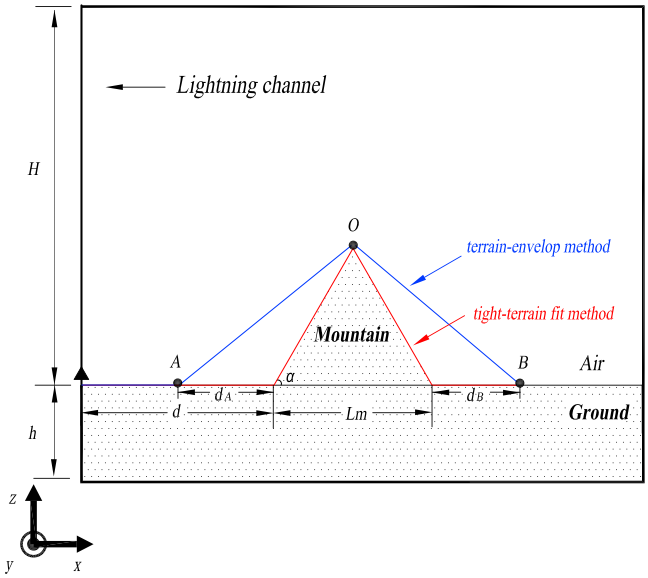

Figure 10. Illustration of two different elongated propagation path methods for the determination of the time delay, the terrain-envelope method marked by the blue line and tight-terrain fit method marked by the red line.

increases as a function of the angle of the mountain. Table 2 further presents the values for the time delay Δt at observation point B, considering different threshold times t_T. Δt represents the difference between the onset times t_{on} obtained with and without considering the presence of the mountain. The values are presented both for perfectly conducting ground and for a finitely conducting ground. It is noted that the time delay Δt depends on the method used to calculate the threshold times. It can be seen all the four methods provide similar results for a perfectly conducting ground/mountain.

On the other hand, for a finitely conducting ground, the time delay Δt shows a slight increase as the observation distance d increases. However, the time delay resulting from the finite ground conductivity appears to be less significant than that caused by the mountainous terrain. It can also be seen that the onset time is nearly insensitive to the mountain conductivity. Moreover, using the time at which the amplitude reaches 10% of the peak provides similar results compared to those corresponding to a threshold time of 20% of the initial rising amplitude of the signal. It is interesting to note that for a finitely conducting ground the onset time obtained from the first time derivative of the magnetic field is larger than those calculated from 10%, 20%, and 50% of the initial rising amplitude of the magnetic field. This is due to the fact that the field time derivative contains more high frequencies compared to the field itself; and therefore, it will be more affected by the finite ground conductivity [see *Cooray*, 2014, chapter 11].

Furthermore, the two simplified methods (terrain-envelope method and tight-terrain fit method) to account for the time delays resulting from the propagation in a mountainous terrain yield time delays that are in reasonable agreement with but always overestimating the results obtained using the full-wave 3-D FDTD approach over the perfectly conducting ground. These two methods represent interesting alternatives to account for the time delay over a nonflat terrain, using available geographical data. For the considered configuration, the terrain-envelope method seems to be more accurate than the tight-terrain fit method. However, more studies involving other geometries are needed to confirm this conclusion.

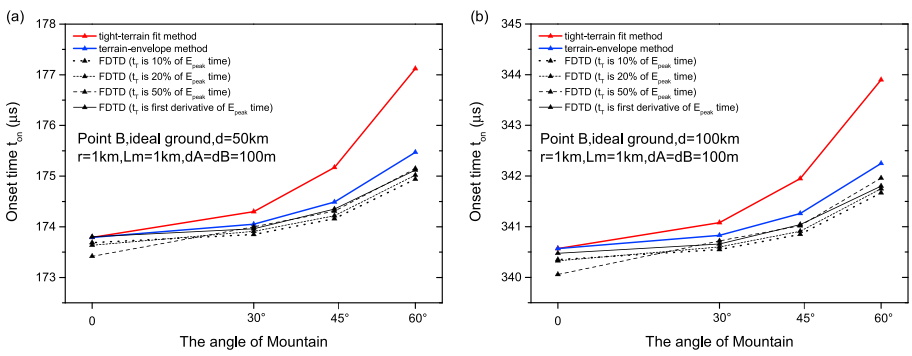

Figure 11. The onset time t_{on} considering different threshold times t_T over a perfectly conducting ground at observation point B, (a) $d = 50$ km, and (b) $d = 100$ km.

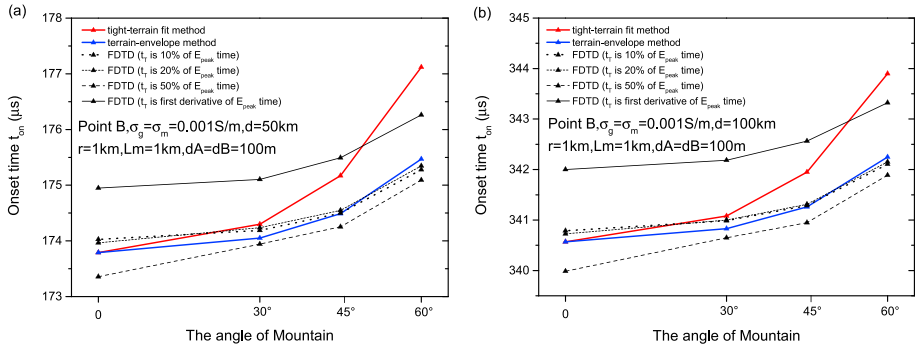

Figure 12. The onset time t_{on} considering different threshold times t_T over a finitely conducting ground ($\sigma_g = 0.001$ S/m and $\varepsilon_{rg} = 10$) at observation point B, (a) $d = 50$ km, and (b) $d = 100$ km.

5. Conclusions and Discussion

We presented an initial analysis of the propagation effects on lightning-radiated electromagnetic fields over mountainous terrain by using a three-dimensional (3-D) finite difference time domain (FDTD) method and a very simple geometrical model for the mountain. We discussed the time delay error in the time-of-arrival (ToA) technique currently used to locate lightning in detection networks. Furthermore, the accuracy of different approximate methods presented in the literature was discussed and tested by using our 3-D FDTD method. It was found that (1) the time delays and amplitudes of the lightning-radiated electromagnetic fields can be significantly affected by the presence of a mountainous terrain and associated diffraction phenomena; (2) for a finitely conducting ground, the time delay shows a slight increase as the observation distance increases, but the time delay resulting from the finite ground conductivity appears to be smaller than that caused by the mountainous terrain. (3) The time delay error associated with the ToA technique depends on the threshold time according to the definition in Figure 1. Onset times calculated using thresholds of 10% and 20% of the peak provide very similar results compared to those corresponding to the peak of the first derivative of the magnetic field. Furthermore, we have assessed the accuracy of two simplified methods (terrain-envelope method and tight-terrain fit method) to account for the time delays resulting from the propagation in a mountainous terrain. It was found that both methods result in time delays that are in reasonable agreement, but for the perfectly conducting ground, always overestimating the results obtained using the full-wave 3-D FDTD approach. These two methods represent interesting alternatives to account for the time delay over a nonflat terrain using

Table 2. Time Delay Δt Resulting From the Presence of the Mountain and Considering Different Threshold Times t_T at Observation Point B[a]

Ground Parameters	d	Angle of the Mountain	Time Delay Δt (s) as a Function of the Threshold Time			
			10% of Peak	20% of Peak	50% of Peak	Peak of the First Derivative
Perfectly conducting ground	1 km	30°	0.32	0.43	0.78	0.24
		45°	0.68	0.79	1.14	0.60
		60°	1.36	1.48	1.83	1.29
	50 km	30°	0.16	0.27	0.49	0.11
		45°	0.47	0.58	0.80	0.42
		60°	1.25	1.38	1.60	1.22
	100 km	30°	0.20	0.27	0.54	0.12
		45°	0.50	0.58	0.85	0.43
		60°	1.32	1.42	1.69	1.27
$\sigma_g = 0.001$ S/m and $\varepsilon_{rg} = 10$	1 km	30°	0.32	0.43	0.86	0.04
		45°	0.68	0.80	1.22	0.40
		60°	1.36	1.49	1.91	1.09
	50 km	30°	0.16	0.27	0.88	−0.71
		45°	0.47	0.58	1.19	−0.40
		60°	1.25	1.38	1.99	0.40
	100 km	30°	0.20	0.27	1.02	−0.99
		45°	0.50	0.58	1.33	−0.69
		60°	1.32	1.42	2.17	0.15

[a]The time delay Δt represents the difference between the onset time t_{on} with and without considering the presence of the mountain.

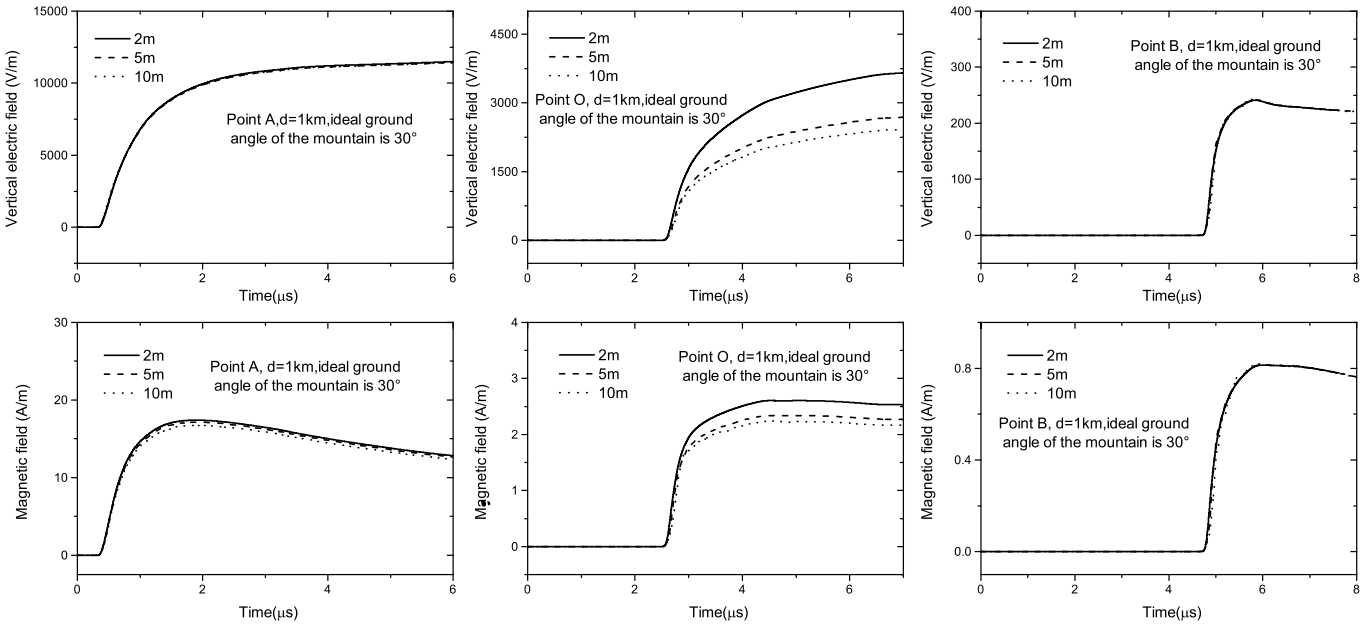

Figure A1. Lightning vertical electric fields and azimuthal magnetic fields at the three observation points (A, O, and B) over a height of 10 m. $d = 1$ km, perfectly conducting ground considering the spatial step of 2 m, 5 m, and 10 m in FDTD simulation.

the terrain model. For the considered configuration, the terrain-envelope method seems to be more accurate than the tight-terrain fit method. However, more studies involving other geometries are needed to confirm this conclusion. In addition, it is worth nothing that the fact that the time delay has errors does not mean that the location will exhibit the same errors since it is the time differences that determine the location.

The evaluation of the resulting location error in an actual lightning detection network is a very complex task that depends on numerous factors (such as the number and location of the sensors), which will be dealt with in future work.

Appendix A: Stair-Stepping Effects on the Electric and Magnetic Field

The stair-stepping effect has been evaluated by comparing results obtained using spatial steps of 2 m, 5 m, and 10 m, which are shown in Figure A1. As can be seen, the accuracy of the numerical results with a spatial step of 10 m is acceptable for observation points in the vicinity of the mountain (A and B). On the top of the mountain, differences of up to about 20% are observed in the amplitude of the E field evaluated with different spatial steps. On the other hand, the magnetic field appears to be nearly invariant when the spatial step is reduced from 10 m down to 2 m.

Figure B1. Idealized lightning channel in the absence of a ground and the far magnetic flux density vector from the current in the channel.

Appendix B: The Effect of the Steepness of the Mountain on the Magnitude of the Magnetic Field at the Top of the Mountain

In this appendix, we use a simplified model to study the effect of the steepness of the mountain on the magnitude of the magnetic field at the top of the mountain, which, as

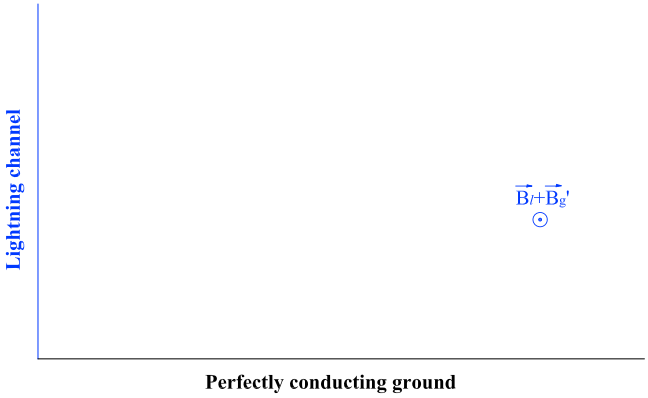

Figure B2. Lightning channel in the presence of the ground. In comparison with the situation in Figure B1, the far magnetic flux density field here is composed of the fields from the lightning channel and from the newly induced currents in the ground.

described in section 4, increases as the angle of the mountain rises up to about 45° and decreases slowly after that. Note that our objective here is to offer a qualitative explanation for this effect through a first-order approximation rather than a rigorous quantitative analysis.

Consider an idealized lightning channel that emits radiation in the absence of a ground as shown in Figure B1.

If we now introduce a perfectly conducting ground, the currents in the ground will act as new sources and the magnetic flux density will now be the sum of the original lightning field and the field from the currents in the ground. The situation is illustrated in Figure B2.

For observation points far from the lightning channel, the total radiated waveform can be approximated as a uniform plane wave. We will now introduce a mountain into the model as shown in Figure B3.

Note that after the introduction of the mountain, the total magnetic flux density still composed of the field from the currents in the lightning channel (which does not change with respect to that for a flat ground) and the field from the ground which is no longer constant since it is dependent on the shape of the mountain. Since only the field due to the currents in the ground depends on the angle of the mountain, we will calculate only that component of the total field.

We model the ground and the mountain in a very simple manner as a single flat wire whose side view is shown in Figure B4.

The current element $I\vec{dl}$ shown in Figure B4 represents the surface currents induced on the conducting metallic wire by the plane wave's horizontal magnetic field produced by the currents in the lightning channel. The induction of these surface currents is required by the magnetic field's boundary condition on the metal surface, and it will ensure that the magnetic field inside the metal is zero.

We will now estimate the magnetic flux density from the ground, $\vec{B}_g'$, at the top of the mountain due to this induced current assuming magnetostatic conditions. Remember that as stated at the top of this appendix our objective is not to calculate the actual magnetic field but to offer a qualitative explanation of the trends observed in the magnetic field as a function of the angle of the mountain.

For the following development, refer to Figure B4. The magnetostatic field from a linear current is given by Biot-Savart's law as

$$\vec{B} = \frac{\mu_0}{4\pi}\int \frac{I\vec{dl}\times r'}{|r'|^3}. \qquad \text{(B1)}$$

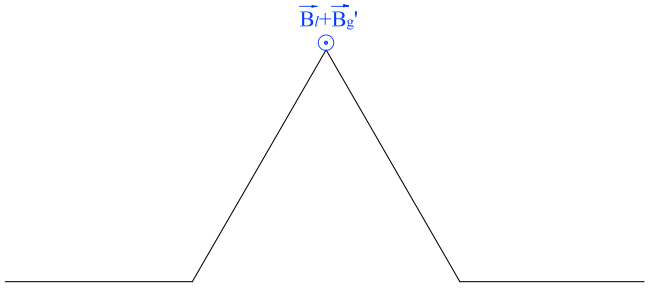

Figure B3. Introduction of the mountain in the model. The magnetic flux density is composed of the field from the lightning channel and the field from the ground.

In our case, the only contribution to the field at the top of the mountain is that of the horizontal section of the wire since the vectors $I\vec{dl}$ and $\vec{r}'$ are parallel along the slope of the mountain, making the vector's cross product equal to zero.

Let us calculate the field produced by the current in the horizontal wire. Since the direction of the cross product in (B1) is constant, we can rewrite that equation as a scalar

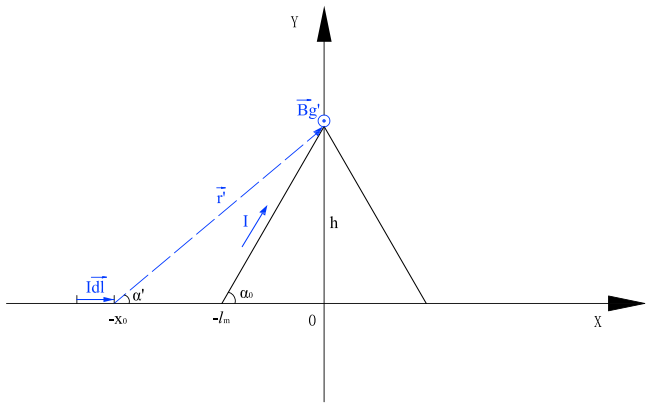

Figure B4. Side view (xoy plane) of the simplified model of the ground and the mountain. The current element $I\vec{dl}$ represents the surface currents induced on the ground. $\vec{B}_{g'}$ is the magnetic flux density from the surface current at the top of the mountain.

$$B = \frac{\mu_0 I}{4\pi}\int \frac{dx}{|r'|^2 \sin(\alpha')}. \tag{B2}$$

Noting that

$$\sin(\alpha') = \frac{h}{(x^2+h^2)^{1/2}},$$
$$r' = (x^2+h^2)^{1/2},$$

and

$$\sin(\alpha_0) = \frac{h}{(l_m^2+h^2)^{1/2}}.$$

Equation (B2) can be readily integrated between $-x_0$ and $-l_m$

$$B = \frac{\mu_0 I}{4\pi}\int_{-x_0}^{-l_m} \frac{h dx}{(x^2+h^2)^{3/2}} = \frac{\mu_0 I}{4\pi h}\frac{x}{(x^2+h^2)^{1/2}}\Big|_{-x_0}^{-l_m} = \frac{\mu_0 I}{4\pi h}\left[\frac{x_0}{(x_0{}^2+h^2)^{1/2}} - \frac{l_m}{(l_m^2+h^2)^{1/2}}\right]. \tag{B3}$$

We now wish to rewrite (B3) in terms of the angle of the mountain α_0. To that end, we note that

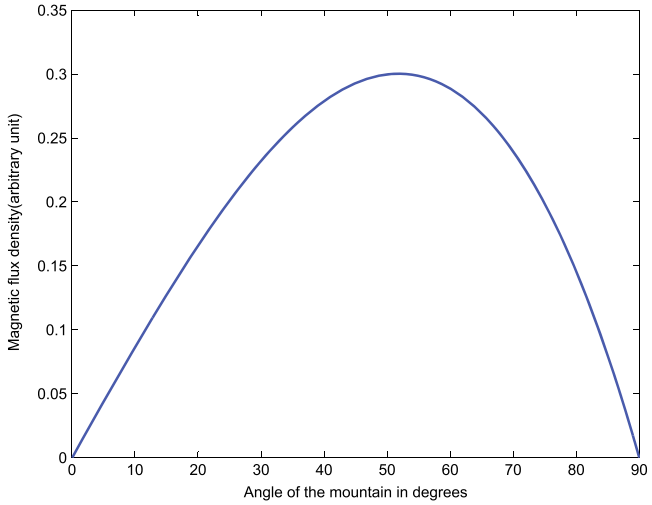

Figure B5. Plot of the magnetic field at the top of the mountain as a function of the angle of the mountain, $\alpha' = 0.1^{\circ}$.

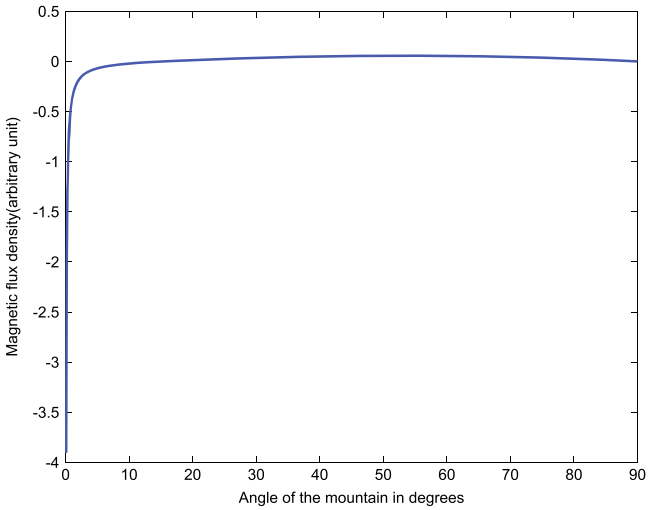

Figure B6. Plot of the magnetic field at the top of the mountain as a function of the angle of the mountain, $\alpha' = 15^{\circ}$.

$$h = l_m \tan(\alpha_0), \tag{B4a}$$

$$h = x_0 \tan(\alpha'). \tag{B4b}$$

Substituting (B4a) and (B4b) into (B3), we get

$$B = \frac{\mu_0 I}{4\pi l_m} \frac{1}{\tan(\alpha_0)} \left[\frac{1}{(1+\tan^2(\alpha'))^{1/2}} - \frac{1}{(1+\tan^2(\alpha_0))^{1/2},} \right. \tag{B5}$$

which can be rewritten as

$$B = \frac{\mu_0 I}{4\pi l_m} \frac{\cos(\alpha') - \cos(\alpha_0)}{\tan(\alpha_0)}. \tag{B6}$$

Equation (B6) gives the magnetic flux density due to the ground at the top of the mountain as a function of the angle of the mountain. Figure B5 shows the plot of this equation using $\alpha' = 0.1°$. A similar, although less pronounced, behavior is observed for other values of α' as illustrated for $\alpha' = 15°$ in Figure B6.

In spite of the limitations as far as the use of quasi-static methods and a flat wire instead of a full surface for the ground and the mountain, the results are in general agreement with the observed trends using full-wave methods. Indeed, as can be seen from Figures B5 and B6, under the assumptions of our simplified model, the magnetic flux density increases as the angle of the mountain increases up to an angle around 50° to 60° and it starts to decrease after that point. This behavior coincides with what was reported in *Paknahad et al.* [2014]. Based on the model, the maximum in the magnetic field versus mountain angle plot can be explained by the angle dependence of the magnetic field from the currents in the ground. However, given the simplicity of the present model, it should only be used as illustrative of the effect.

Acknowledgments
This research was supported by National Key Basic Research Program of China grant (2014CB441405), China Commonweal Industry Research Project (GYHY201306078), the National Natural Science Foundation of China (41275043 and 40875016), the Swiss National Science Foundation (grant 200021_147058), and China Scholarship Council (CSC). We do not use any data in the paper, and the presented analysis is based exclusively on numerical simulations.

References

Baba, Y., and V. A. Rakov (2003), On the transmission line model for lightning return stroke representation, *Geophys. Res. Lett.*, *30*(24), 2294, doi:10.1029/2003GL018407.

Baba, Y., and V. A. Rakov (2014), Applications of the FDTD method to lightning electromagnetic pulse and surge simulations, *IEEE Trans. Electromagn. Compat.*, *56*(6), 1506–1521, doi:10.1109/TEMC.2014.2331323.

Caligaris, C., F. Delfino, and R. Procopio (2008), Cooray–Rubinstein formula for the evaluation of lightning radial electric fields: Derivation and implementation in the time domain, *IEEE Trans. Electromagn. Compat.*, *50*(1), 194–197, doi:10.1109/TEMC.2007.913226.

Cooray, V. (1987), Effects of propagation on the return stroke radiation fields, *Radio Sci.*, *22*(5), 757–768.

Cooray, V. (2009), Propagation effects due to finitely conducting ground on lightning-generated magnetic fields evaluated using Sommerfeld's integrals, *IEEE Trans. Electromagn. Compat.*, *51*(3), 526–531, doi:10.1109/TEMC.2009.2019759.

Cooray, V. (2014), *The Lightning Flash*, 2nd ed., Inst. of Eng. and Technol., London.

Cooray, V., and Y. Ming (1994), Propagation effects on the lightning-generated electromagnetic fields for homogeneous and mixed sea-land paths, *J. Geophys. Res.*, *99*, 10,641–10,652, doi:10.1029/93JD03277.

Cooray, V., M. Fernando, T. Sörensen, T. Götschl, and A. Pedersen (2000), Propagation of lightning generated transient electromagnetic fields over finitely conducting ground, *J. Atmos. Sol. Terr. Phys.*, *62*(7), 583–600, doi:10.1016/S1364-6826(00)00008-0.

Cummins, K. L., M. J. Murphy, E. A. Bardo, W. L. Hiscox, R. B. Pyle, and A. E. Pifer (1998), A combined TOA/MDF technology upgrade of the US National Lightning Detection Network, *J. Geophys. Res.*, *103*, 9035–9044.

Cummins, K. L., M. Murphy, J. Cramer, W. Scheftic, N. Demetriades, and A. Nag (2010), Location accuracy improvements using propagation corrections: A case study of the US National Lightning Detection Network, paper presented at 21st International Lightning Detection Conference, Orlando, Fla.

Delfino, F., R. Procopio, M. Rossi, F. Rachidi, and C. A. Nucci (2008), Lightning return stroke current radiation in presence of a conducting ground: 2. Validity assessment of simplified approaches, *J. Geophys. Res.*, *113*, D05111, doi:10.1029/2007JD008567.

Diendorfer, G. (2007), Lightning location systems (LLS), paper presented at IX International symposium on lightning protection. Foz do Iguaçu, Brazil.

Honma, N., F. Suzuki, Y. Miyake, M. Ishii, and S. Hidayat (1998), Propagation effect on field waveforms in relation to time-of-arrival technique in lightning location, *J. Geophys. Res.*, *103*, 14,141–14,145, doi:10.1029/97JD02625.

Honma, N., K. L. Cummins, M. J. Murphy, A. E. Pifer, and T. Rogers (2013), Improved lightning locations in the Tohoku Region of Japan using propagation and waveform onset corrections, *IEEJ Trans. Power Energy*, *133*(2), 195–202, doi:10.1541/ieejpes.133.195.

Li, D., Q. Zhang, T. Liu, and Z. Wang (2013), Validation of the Cooray-Rubinstein (C-R) formula for a rough ground surface by using three-dimensional (3-D) FDTD, *J. Geophys. Res. Atmos.*, *118*, 12,749–12,754, doi:10.1002/2013JD020078.

Li, D., Q. Zhang, Z. Wang, and T. Liu (2014), Computation of lightning horizontal field over the two-dimensional rough ground by using the three-dimensional FDTD, *IEEE Trans. Electromagn. Compat.*, *56*(1), 143–148, doi:10.1109/TEMC.2013.2266479.

Li, D., F. Rachidi, M. Rubinstein, J. Paknahad, K. Sheshyekani, Q. Zhang, and Z. Wang (2015), Propagation effects on lightning magnetic fields over hilly and mountainous terrain, in *2015 IEEE International Symposium on Electromagnetic Compatibility (EMC)*, pp. 1436–1440, IEEE, Dresden, Germany, doi:10.1109/ISEMC.2015.7256384.

Lojou, J., N. Honma, K. L. Cummins, R. K. Said, and N. Hembury (2011), Latest developments in global and total lightning detection, paper presented at 7th Asia-Pacific International Conference on Lightning (APL), Chengdu, China, 1–4 Nov.

Nucci, C. A., and F. Rachidi (1989), Experimental validation of a modification to the transmission line model for LEMP calculation, paper presented at 8th Symposium and Technical Exhibition on Electromagnetic Compatibility, Zurich, Switzerland.

Nucci, C. A., C. Mazzetti, F. Rachidi, and M. Ianoz (1988), On lightning return stroke models for LEMP calculations, paper presented at 19th International Conference on Lightning Protection, Graz, Austria.

Paknahad, J., K. Sheshyekani, M. Hamzeh, and F. Rachidi (2014), Lightning electromagnetic fields and their induced voltages on overhead lines: The effect of a non-flat lossy ground, paper presented at 32nd International Conference on Lightning Protection (ICLP), IEEE, Shanghai, China.

Passi, R. M., and R. E. López (1989), A parametric estimation of systematic errors in networks of magnetic direction finders, *J. Geophys. Res.*, *94*, 13,319–13,328, doi:10.1029/JD094iD11p13319.

Rachidi, F., and C. A. Nucci (1990), On the Master, Uman, Lin, Standler and the modified transmission line lightning return stroke current models, *J. Geophys. Res.*, *95*, 20,389–20,393, doi:10.1029/JD095iD12p20389.

Rachidi, F., W. Janischewskyj, A. M. Hussein, C. A. Nucci, S. Guerrieri, B. Kordi, and J. S. Chang (2001), Current and electromagnetic field associated with lightning-return strokes to tall towers, *IEEE Trans. Electromagn. Compat.*, *43*(3), 356–367, doi:10.1109/15.942607.

Roden, J. A., and S. D. Gedney (2000), Convolutional PML (CPML): An efficient FDTD implementation of the CFS-PML for arbitrary media, *Microwave Opt. Technol. Lett.*, *27*(5), 334–338, doi:10.1002/1098-2760(20001205)27:5<334::AID-MOP14>3.0.CO;2-A.

Rubinstein, M. (1996), An approximate formula for the calculation of the horizontal electric field from lightning at close, intermediate, and long range, *IEEE Trans. Electromagn. Compat.*, *38*(3), 531–535, doi:10.1109/15.536087.

Schulz, W. (1997), Performance evaluation of lightning location systems, PhD thesis, Technical Univ. of Vienna, Vienna, Austria.

Schulz, W., and G. Diendorfer (2000), Evaluation of a lightning location algorithm using an elevation model, paper presented at 25th International Conference on Lightning Protection (ICLP), Rhodos, Greece.

Shoory, A., A. Mimouni, F. Rachidi, V. Cooray, and M. Rubinstein (2011), On the accuracy of approximate techniques for the evaluation of lightning electromagnetic fields along a mixed propagation path, *Radio Sci.*, *46*, RS2001, doi:10.1029/2010RS004480.

Shoory, A., F. Rachidi, and V. Cooray (2012), Propagation effects on electromagnetic fields generated by lightning return strokes: Review of simplified formulas and their validity assessment, in *Lightning Electromagnetics*, *Rep. EPFL-CHAPTER-181767*, chap. 12, pp. 485–513, IET, London, U. K.

Taflove, A., and S. C. Hagness (1995), *Computational Electrodynamics: the Finite-Difference Time-Domain Method*, 2nd ed., Artech House, Norwood, Mass.

Taflove, A., and S. C. Hagness (2005), *Computational Electrodynamics: The Finite-Difference Time-Domain Method*, Artech House, Norwood, Mass.

Uman, M. A., D. K. McLain, and E. P. Krider (1975), The electromagnetic radiation from a finite antenna, *Am. J. Phys.*, *43*(1), 33–38.

Watts, M. (2003), Perfect plane-wave injection into a finite FDTD domain through teleportation of fields, *Electromagnetics*, *23*(2), 187–201.

Zhang, Q., J. Yang, X. Jing, D. Li, and Z. Wang (2012a), Propagation effect of a fractal rough ground boundary on the lightning-radiated vertical electric field, *Atmos. Res.*, *104*, 202–208.

Zhang, Q., J. Yang, D. Li, and Z. Wang (2012b), Propagation effects of a fractal rough ocean surface on the vertical electric field generated by lightning return strokes, *J. Electrost.*, *70*(1), 54–59.